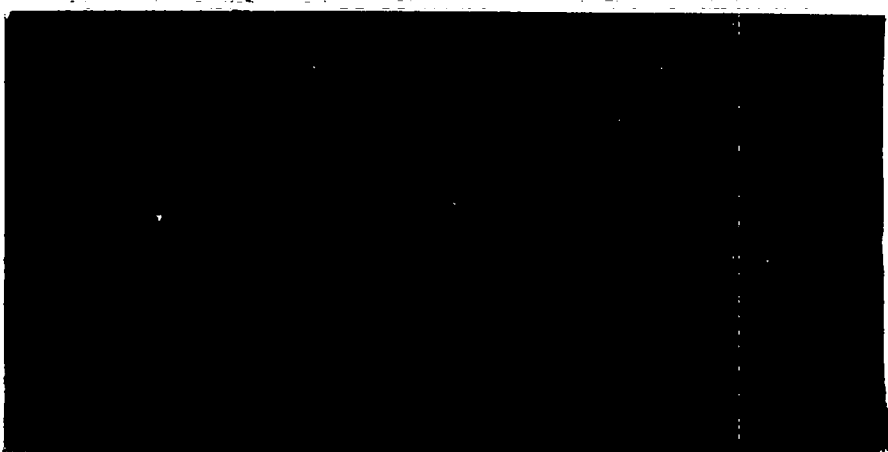


C. 19

LOS ALAMOS SCIENTIFIC LABORATORY

OF THE UNIVERSITY OF CALIFORNIA
LOS ALAMOS, NEW MEXICO



LOS ALAMOS NATL. LAB. LIBS
3 9338 00353 5654

CONTRACT W-7405-ENG. 36 WITH THE
U.S. ATOMIC ENERGY COMMISSION

FOR REFERENCE

NOT TO BE TAKEN FROM THIS ROOM

CAT. NO. 1935

LIBRARY BUREAU



C. 19

LOS ALAMOS SCIENTIFIC LABORATORY
of the
UNIVERSITY OF CALIFORNIA

Report written:
January 19, 1955

Report distributed: OCT 18 1955

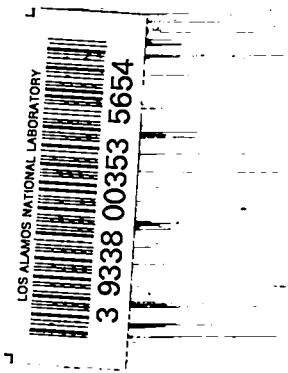
LA-1930

A NUMERICAL METHOD FOR TREATING FLUID FLOW
IN THE PRESENCE OF SHOCKS

by

Rolf Landshoff

PHYSICS



ABSTRACT

This report describes a numerical method to calculate the flow of a compressible fluid in the presence of shocks. It is related to the method of von Neumann and Richtmyer⁽¹⁾ and, to a lesser extent, to that of P. Lax.⁽²⁾ This method permits a number of variations which were compared by testing them on some analytically known one-dimensional flow patterns. The calculations were carried out on the Los Alamos "MANIAC."

CONTENTS

	Page
Abstract	2
1. General Remarks	5
2. Development of Method	8
3. Analytical Solution of Test Problems	13
4. Numerical Tests	18
References	41

TABLES

Table 1. Shock Relations for $\gamma = 1.4$ (Cases A and B).	14
Table 2. Rarefaction Wave Relations for $\gamma = 1.4$ (Case C).	17
Table 3. Shock Tube Relations for $\gamma = 1.4$ (Case D).	19

ILLUSTRATIONS

Fig. 1. Positions of points 1 and 2.	8
Fig. 2. Fan in the $x - t$ plane separating two regions of uniform conditions	15
Fig. 3. The x, t diagram for the shock tube problem.	16
Fig. 4. Typical shock profiles with only one type of viscosity.	21
Fig. 5. Relative errors vs. St	23
Fig. 6. Lines of constant ϵ_3 in the c_1, c_2 plane.	24
Fig. 7. Shock width vs. c_2	26
Fig. 8. Comparison of viscosity with steady state theory.	27

Fig. 9.	Ratio of actual density in the first zone to theoretical density for the steady state solution.	29
Fig. 10.	Density profiles for selected combinations of c_1 and c_2	31
Fig. 11.	Pressure profile for rarefaction wave	33
Fig. 12.	Density near piston end of rarefaction fan.	34
Fig. 13.	Density near head of rarefaction wave	35
Fig. 14.	Values of q determined by method 2.	36
Fig. 15.	Density in shock tube.	38
Fig. 16.	Density near plateau	39
Fig. 17.	Error of the average density and the average error of the density in the shock region	40

1. General Remarks

The one-dimensional hydrodynamic equations can be written in the Lagrangian form

$$\rho_0 \frac{du}{dt} = - \frac{\partial p}{\partial x} , \quad (1)$$

$$\rho_0 \frac{\partial v}{\partial t} = \frac{\partial u}{\partial x} , \quad (2)$$

and

$$\frac{\partial p}{\partial t} = - (\rho_0 w)^2 \frac{\partial v}{\partial t} = - \rho_0 w^2 \frac{\partial u}{\partial x} ; \quad (3)$$

where

u = velocity,

p = pressure,

v = specific volume,

ρ_0 = initial density,

x = initial position of a particle,

and where

$$(\rho_0 w)^2 = \left(\frac{\partial S}{\partial v} \right) / \left(\frac{\partial S}{\partial p} \right)$$

in which

S = entropy.

The first two of these equations are in the form of conservation

theorems and can, with the aid of Green's theorem, be integrated in a shock region. The third equation is clearly wrong in the presence of a shock. Nevertheless, we use it to expand p for use in eq.(1):

$$p = p(x,0) - \rho_0 w^2 \frac{\partial u}{\partial x} t \quad . \quad (4)$$

Upon integrating eq.(1) to a small value of $t = \delta t$, we get

$$u(x, \delta t) = u(x,0) - \frac{1}{\rho_0} \frac{\partial}{\partial x} \left[p(x,0) - \frac{\rho_0 w^2}{2} \frac{\partial u}{\partial x} \delta t \right] \delta t \quad . \quad (5)$$

An alternative method of integration is due to Riemann, who defined a quantity

$$\sigma = - \int \rho_0 w \, dv \quad (6)$$

and showed that the quantities $u \pm \sigma$ remain constant along the so-called characteristics defined as the lines

$$\frac{dx}{dt} = \pm w. \quad (7)$$

Therefore, if x_1 and $x_2 > x_1$ are two points on the x -axis and if the forward characteristics through x_1 and the backward characteristics through x_2 meet a little time later at a point x , we have at that point

$$u + \sigma = u_1 + \sigma_1 \quad (8)$$

and

$$u - \sigma = u_2 - \sigma_2 \quad (9)$$

which yield

$$u = \frac{1}{2} (u_1 + u_2) + \frac{1}{2} (\sigma_1 - \sigma_2). \quad (10)$$

This solution is related to the construction of solutions of the wave equation by Huygen's principle. This principle* states that a solution in a space of an odd number of dimensions depends only on the starting values at the border of the domain of dependence. In an even dimensional space, it depends also on the interior of this domain although the influence of the border is still the stronger. In no case do points outside of the domain of dependence have any effect.

* A detailed discussion can be found in (3), Chapter 6, para. 5.3.

2. Development of Method

The computing scheme proposed here uses a rectangular lattice (x_i, t_n) . Velocities u_i^n and displacements X_i^n are defined at the lattice points, whereas specific volumes $v_{i+1/2}^n$ and pressures $p_{i+1/2}^n$ are defined between them as indicated by the $i+1/2$.

If eq.(10) is applied to calculate u_i^{n+1} , the points 1 and 2 lie as indicated in Fig. 1 and can be computed from eq.(7).

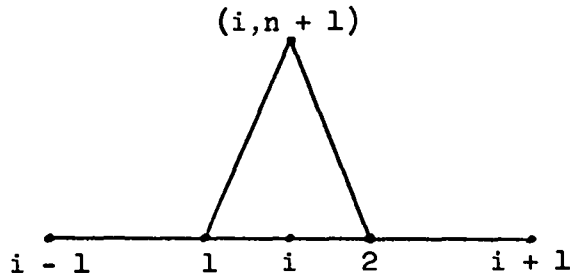


Fig. 1

One can show that the second term in eq.(10), if expressed in terms of quantities defined in the latter scheme, is

$$\frac{\sigma_1 - \sigma_2}{2} = \frac{2 (p_{i-1/2}^n - p_{i+1/2}^n)}{\rho_0 (x_{i+1} - x_{i-1})} \delta t. \quad (11)$$

This expression is the same as one would get from the pressure derivative term in eq.(5). The first term in eq.(10) can be expressed in more than one way. The choice is introduced by using different interpolation schemes for expressing u_1 and u_2 . If one fits u at the three points x_{i-1} , x_i , and x_{i+1} by a parabola which has its axis parallel to the u -axis and if one fits w by a

line at $x_i - 1/2$ and $x_i + 1/2$, then one finds that the leading terms are

$$\frac{u_1 + u_2}{2} = u_i^n + \frac{2(q_i^n - 1/2 - q_{i+1/2}^n)}{\rho_0(x_{i+1} - x_{i-1})} \delta t, \quad (12)$$

where

$$q_{i+1/2}^n = \frac{1}{2} \rho_0 (w_{i+1/2}^n)^2 \frac{(u_i^n - u_{i+1}^n)}{x_{i+1} - x_i} \delta t. \quad (13)$$

This is the same expression one would get from eq.(5). If one fits u by two straight lines between adjacent points and w in each interval by its central value, one obtains eq.(12) but with a different q :

$$q_{i+1/2}^n = \frac{1}{2} \rho_0 w_{i+1/2}^n (u_i - u_{i+1}). \quad (14)$$

One might think of other combinations of interpolating the two quantities u and w , but the two which were chosen have the virtue of leading to an equation of the type (12), which ensures the conservation of momentum.

The transcription of eq.(2), which expresses the conservation of mass, can be done as follows. We introduce the position x_i^n and integrate:

$$x_i^{n+1} - x_i^n = \frac{1}{2} (u_i^{n+1} + u_i^n) \delta t \quad (15)$$

and calculate the volume from

$$\rho_0 v_{i+1/2}^n = x_{i+1}^n - x_i^n . \quad (16)$$

As was pointed out earlier, eq.(3) is not in the form of a conservation theorem. In order to put the conservation of energy into evidence, we write

$$\rho_0 \frac{\partial}{\partial t} \left(E + \frac{u^2}{2} \right) = - \frac{\partial}{\partial x} (pu) , \quad (17)$$

where $E(p,v)$ is the internal energy. One has to exercise care in performing averages in the transcription of this equation into difference equation form, for u , which occurs on both sides of eq. (17) is not defined at the half points as are p and E . It turns out that one can obtain a much simpler form if one alters eq.(17) by replacing p on the right hand side by $p + q$ as was done in Ref. 1. If one does not bother to center the right hand side of eq.(15) in time but replaces it by its value at t_n , then the transcribed equation can be put into the form:

$$E_{i+1/2}^{n+1} - E_{i+1/2}^n + (p_{i+1/2}^n + q_{i+1/2}^n)(v_{i+1/2}^{n+1} - v_{i+1/2}^n) = 0 . \quad (18)$$

This equation does not exhibit the conservation, but it possesses it

nevertheless if one uses it in conjunction with eqs.(10), (11), and (12). Formally, the above equations look like they contain a viscosity term if one uses eq.(14) for q ; and indeed, similar to the viscosity method of von Neumann and Richtmyer (Ref. 1), they lend themselves to the treatment of not too strong shocks. On comparing the results obtained by using for q an expression q_1 which is linear in Δu as given by eq.(14) or an expression q_2 which is quadratic in Δu as suggested in Ref. 1, the following was found (Fig.4, p.21). The use of q_1 gave a fairly large overshoot behind the shock which damped out quite rapidly in the wake of the shock. The use of q_2 gave a smaller initial overshoot, but it damped out slower. It seemed advisable, therefore, to use a combination of q_1 and q_2 in order to get both a small overshoot and a rapid damping. Either one does some violence to the equations, which has the effect of smearing out discontinuities such as shockfronts, interfaces, or heads of rarefaction waves and of introducing disturbances at boundaries which will be discussed in more detail later on in this paper.

It is therefore desirable to keep this violence at a minimum, and this may be done in a number of ways. The q_2 suggested by von Neumann and Richtmyer is of the form

$$q_2 = -c_2 \frac{\Delta u |\Delta u|}{V} \quad , \quad (19)$$

where

$$\Delta u = u_1 + 1/2 - u_1 - 1/2 \quad . \quad (20)$$

It was recognized quite long ago by the people who used this method that there was no need for a viscosity term for positive Δu , and one often finds it replaced by zero for that range. This "spliced q_2 " has a continuous first derivative. One can also adjust the parameter c_2 ; and, in the absence of q_1 , $c_2 = 2$ is about right to handle most cases. Of the two expressions given for q_1 , the one in eq.(13) is, in the absence of discontinuities, correct to one order higher in δt than the one given by eq.(14). One can reduce the violence done by applying eq.(14) alone by mixing the two expressions, i.e.,

$$q_1 = -\frac{1}{2} \rho_0^w \Delta u \left[c_1 + (1 - c_1) \frac{\delta t}{\Delta x} \right], \quad (21)$$

with the indices as in eqs.(13) and (14). Aside from "method 1", which consists of the continuation of q_1 given by eq.(21), and the spliced q_2 , we shall also test "method 2", which comes closer to the requirement of having no viscosity for positive Δu . In method 2, we use $q_1 + q_2$, with q_2 given by eq.(19), up to the value of Δu where $q_1 + q_2$ reaches its minimum and that minimum for values of Δu beyond. In this method, $q_1 + q_2$ is also a smooth function of Δu .

3. Analytical Solution of Test Problems

The above methods were tested on a gas for which

$$E = p v / (\gamma - 1) \quad , \quad (22)$$

with $\gamma = 1.4$. The specific cases to which tests were applied were as follows:

A. A shock which is induced by a piston of constant velocity u_0 running into material of constant $V = V_1$ and at rest. The theory leads to a shock with constant values of $u = u_2 = u_0$, $V = V_2 = \frac{V_1}{\eta}$, $p = p_2 = \xi p_1$ between the piston and a shock front going with the constant velocity D . We obtain (with $\mu = \frac{\gamma + 1}{\gamma - 1}$)

$$\frac{u^2}{p_1 V_1} = (\mu - 1) \frac{(\xi - 1)^2}{\mu \xi + 1} \quad , \quad (23)$$

$$\eta = \frac{\mu \xi + 1}{\mu + \xi} \quad , \quad (24)$$

and

$$D = \sqrt{\gamma p_1 V_1} \cdot \sqrt{1 + \frac{\mu}{\mu + 1} (\xi - 1)} \quad . \quad (25)$$

A few useful numerical values pertaining to the actual test problems are collected in Table 1.

TABLE 1

Shock Relations for $\gamma = 1.4$ (Cases A and B)

$u / \sqrt{p_1 V_1}$	ξ	η	ξ/η^γ	$D / \sqrt{p_1 V_1}$	$\sqrt{\gamma \xi \eta}$
4	21.303	4.718	2.427	5.076	11.86
16	309.4	5.889	25.88	19.27	50.50
3.862	20	4.654	2.323	4.919	11.41
16.275	320	5.893	26.70	19.60	51.38

B. Same as A, but with the piston driven by a constant pressure. The theory is the same as under A.

C. A rarefaction wave induced by a piston receding with a negative velocity u_0 . This leads to a simple wave as discussed, for example, in Ref. 4, para. 40. In this solution one has a fan in the $x - t$ plane separating two regions of uniform conditions.

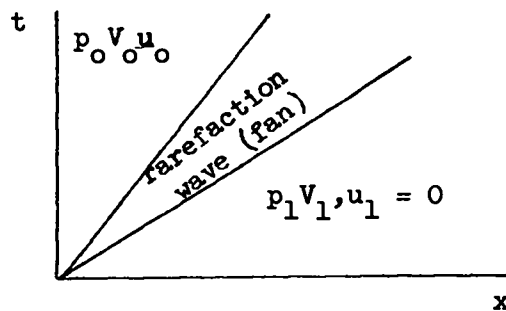


Fig. 2

One obtains $p_0 = \xi p_1$ and $v_0 = \frac{v_1}{\eta}$ from

$$\eta = \left(1 - \frac{\gamma - 1}{2\sqrt{\gamma}} \frac{|u_0|}{\sqrt{p_1 v_1}} \right)^{\frac{2}{\gamma - 1}} \quad (26)$$

and

$$\xi = \eta^\gamma \quad (27)$$

In the fan we have

$$\frac{x}{t} = v_1 \sqrt{\gamma \frac{p}{v}} \quad , \quad (28)$$

and, with pV^{γ} constant as in eq. (27),

$$\frac{p}{p_1} = \left(\frac{x/t}{\sqrt{p_1 v_1}} \right)^{\frac{2}{\gamma+1}} \quad (29)$$

The speed of the front and rear end of the fan are obtained from (28) by substituting p_1, V_1 and p_0, V_0 respectively. Some numerical values are found in Table 2.

D. The shock tube problem (see Ref. 4, para. 80). Each of two media in contact is initially at rest and at constant density and pressure, but the two densities and pressures are different. Fig. 3 gives the x, t diagram.

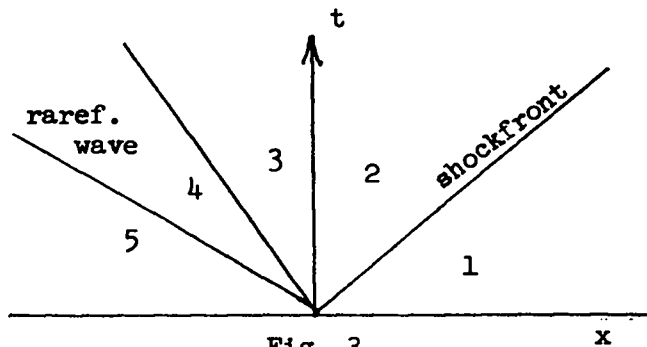


Fig. 3

Between regions 2 and 3 is what Ref. 4 calls a contact discontinuity, i.e., p and u are continuous but V is not. We define $\xi = \frac{p_2}{p_1}$, $\eta = \frac{v_1}{v_2}$, and $X = p_5/p_1$. X is given, ξ and η are to be found. We can express

$$u_2 = \sqrt{\frac{(\mu-1) p_1 v_1}{\mu \xi + 1}} (\xi - 1) \quad (30)$$

$$u_3 = \frac{2\sqrt{\gamma}}{\gamma-1} \sqrt{p_5 v_5} \left(1 - \left(\frac{\xi}{X}\right)^{\frac{\gamma-1}{2\gamma}} \right) \quad (31)$$

TABLE 2

Rarefaction Wave Relations for $\gamma = 1.4$ (Case C)

$u / \sqrt{p_1 V_1}$	ξ	η	$\sqrt{\xi \eta}$
- 1	.274	.396	.390
- 4	.000374	.00356	.00136

and find ξ by equation $u_2 = u_3$. η and the shock velocity D can then be found from eqs. (24) and (25) and v_3 from

$$v_3 = v_5(x/\xi)^{1/\gamma} \quad (32)$$

Conditions in the fan are given by relations like (28) and (29) with p_1 , v_1 , and x replaced by p_5 , v_5 , and $-x$. Some numerical values are given in Table 3.

4. Numerical Tests

The method of integration was tested on the four cases treated analytically in the previous section. Equations (15) and (16) were used for conservation of mass. Expressions (11) and (12) are entered into eq. (10) to give what was used for the conservation of momentum:

$$u_i^{n+1} = u_i^n + \frac{2(p_{i-1/2}^n + q_{i-1/2}^n - p_{i+1/2}^n - q_{i+1/2}^n) \delta t}{\rho_0(x_{i+1} - x_{i-1})} \quad (33)$$

The equation of state (22) is entered into eq. (18) to give the equations which were used for the conservation of energy:

TABLE 3

Shock Tube Relations for $\gamma = 1.4$ (Case D)

p_5/p_1	p_3/p_5	ρ_3/ρ_5	ρ_2/ρ_5	$u_3/\sqrt{p_1 V_1}$	$D/\sqrt{p_1 V_1}$
2	.7009	.7758	.6357	.2929	1.372
16	.2142	.3328	.1430	1.082	2.077
32	.1381	.2431	.08251	1.458	2.345
64	.08711	.1749	.04650	1.743	2.625
128	.05368	.1259	.02563	2.020	2.906
512	.01923	.05946	.007404	2.552	3.466

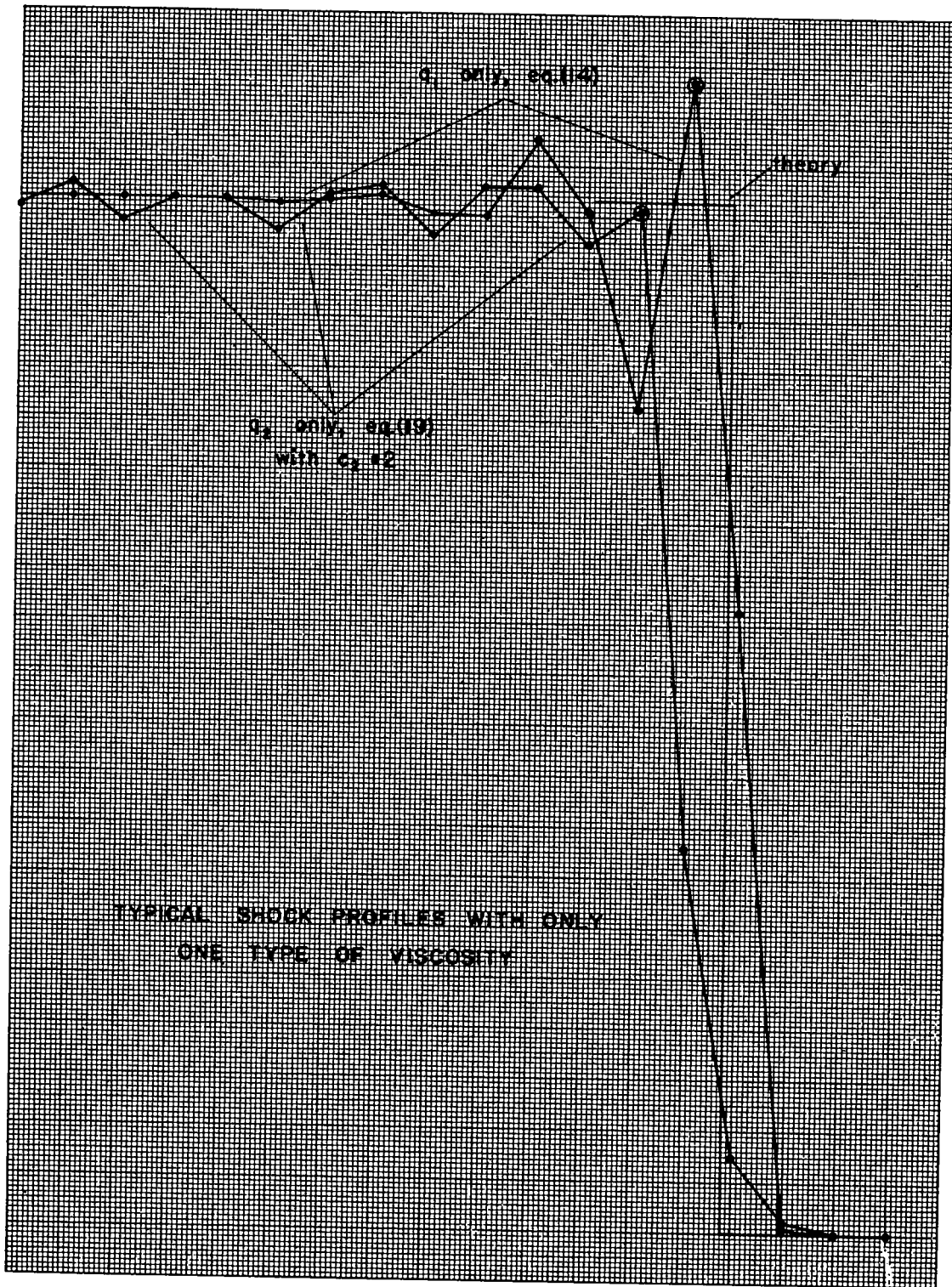
$$p_{i+1/2}^{n+1} = y p_{i+1/2}^n + (\gamma - 1)(y - 1) (p_{i+1/2}^n + q_{i+1/2}^n) , \quad (34)$$

where

$$y = \frac{v_{i+1/2}^n}{v_{i+1/2}^{n+1}} \quad (35)$$

The tests were carried out with $\gamma = 1.4$. Runs were made in the one-medium cases A, B and C, with 30 and in the two-medium case D with 60 mass points.

In the cases A and B, which test the method for its treatment of shocks, the problems were run without interruption up to a time where one can still run 32 more cycles before the shock reaches the last mass point. At this time a printout was made of all physical variables and in the remaining 32 cycles a fluctuation calculation is carried out. First, the shocked region is located by going from the last mass point backwards and testing for the first pressure maximum. In the two runs presented in Fig. 4, for example, these are the encircled points. From there back to the piston, the average pressure \bar{p} as well as the maximum and the mean value of the square deviation $\Delta p^2 = (p - \bar{p})^2$ are calculated in each cycle. Following this through 32 cycles the time averages $\bar{\bar{p}}$, $\overline{(\bar{p} - \bar{p})^2}$, $\overline{\Delta p^2}$, and $\overline{\Delta p_{\max}^2}$ were calculated and the absolute maximum $\Delta p_{\max \max}^2$ was recorded. Let us define relative errors as follows:



TYPICAL SHOCK PROFILES WITH ONLY
ONE TYPE OF VISCOSITY

Fig. 4 Typical shock profiles with only one type of viscosity.

$$\epsilon_1 = \frac{\bar{p} - \xi p_1}{\bar{p}}, \quad \epsilon_2 = \sqrt{(\bar{p} - \bar{p})^2} / \bar{p}, \quad \epsilon_3 = \sqrt{\Delta p^2} / \bar{p},$$

$$\epsilon_4 = \sqrt{\Delta p_{\max}^2} / \bar{p}, \quad \epsilon_5 = \sqrt{p_{\max}^2} / \bar{p}.$$

In Fig.5, these five relative errors are plotted as a function of δt for a typical case. Also indicated is the Courant-Friedrichs-Lewy limit, which is given by the relation $\sqrt{\gamma \xi \eta p_1 v_1} \delta t_{\text{CFL}} / \delta x = 1$. Below about $\frac{\delta t_{\text{CFL}}}{2}$, ϵ_1 is exceedingly small and positive or negative without any apparent correlation to any other factors. The quantities $\epsilon_2, \epsilon_3,$ and ϵ_4 have constant ratios for all cases considered, except for small random variations. ϵ_5 / ϵ_3 is generally somewhat larger for small values of δt . This is, however, not too significant; and for judging the merit of different combinations of c_1 and c_2 , we shall consider only one of the five ϵ 's, namely ϵ_3 .

One can obtain some feeling for the merit of different combinations of c_1 and c_2 in calculating this type of flow by constructing lines of constant ϵ_3 in the c_1, c_2 plane. Such diagrams are presented for two shocks of different strength in Fig. 6. Optimal smoothing occurs for $c_1 = 1$ and for values of c_2 ranging about from 1 to 2. If optimal smoothing were the only criterion for choosing the parameters c_1 and c_2 , the problem would be solved with the above observation. However, too much smoothing has also some undesirable features. Two of

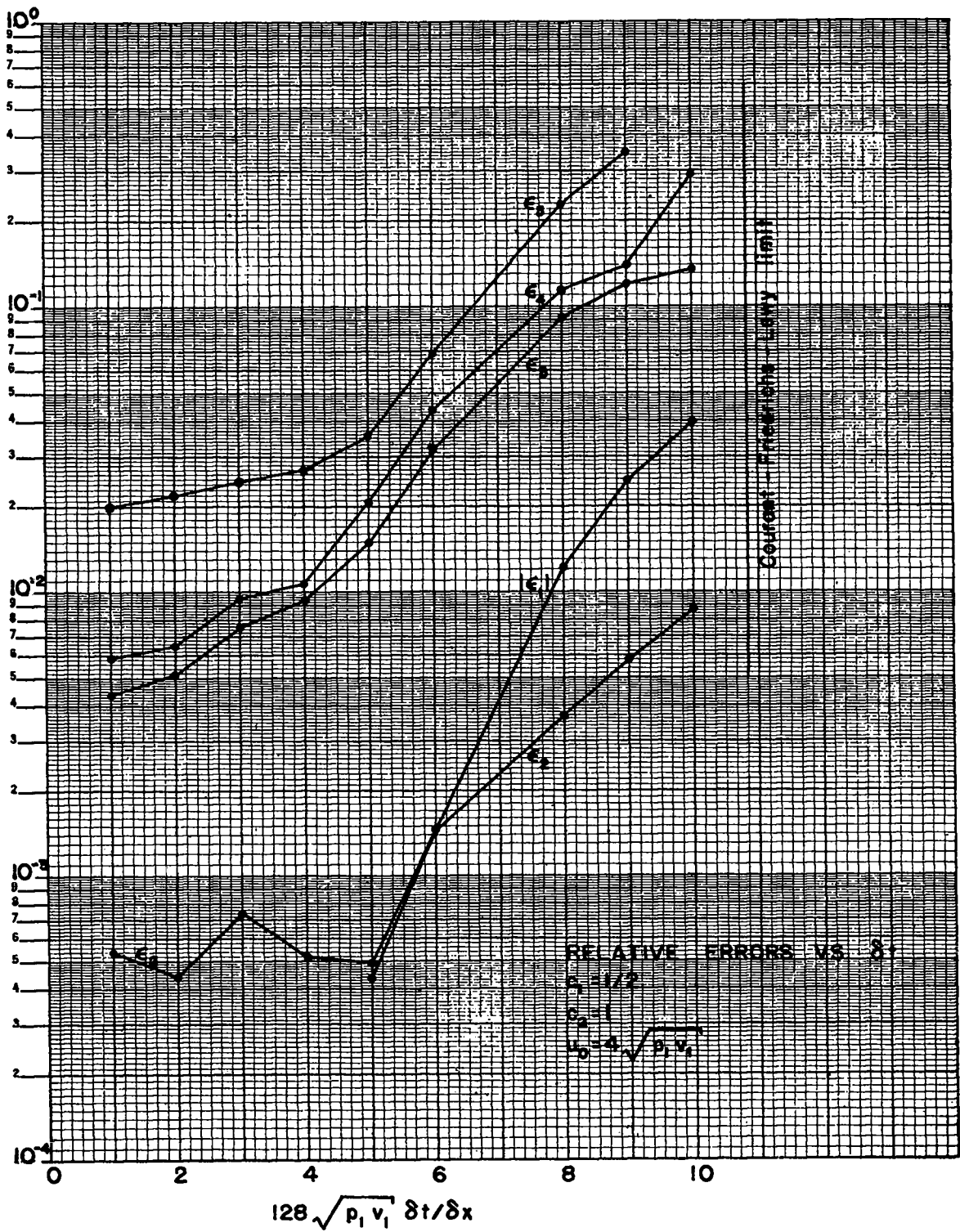


Fig. 5 Relative errors vs. δt .

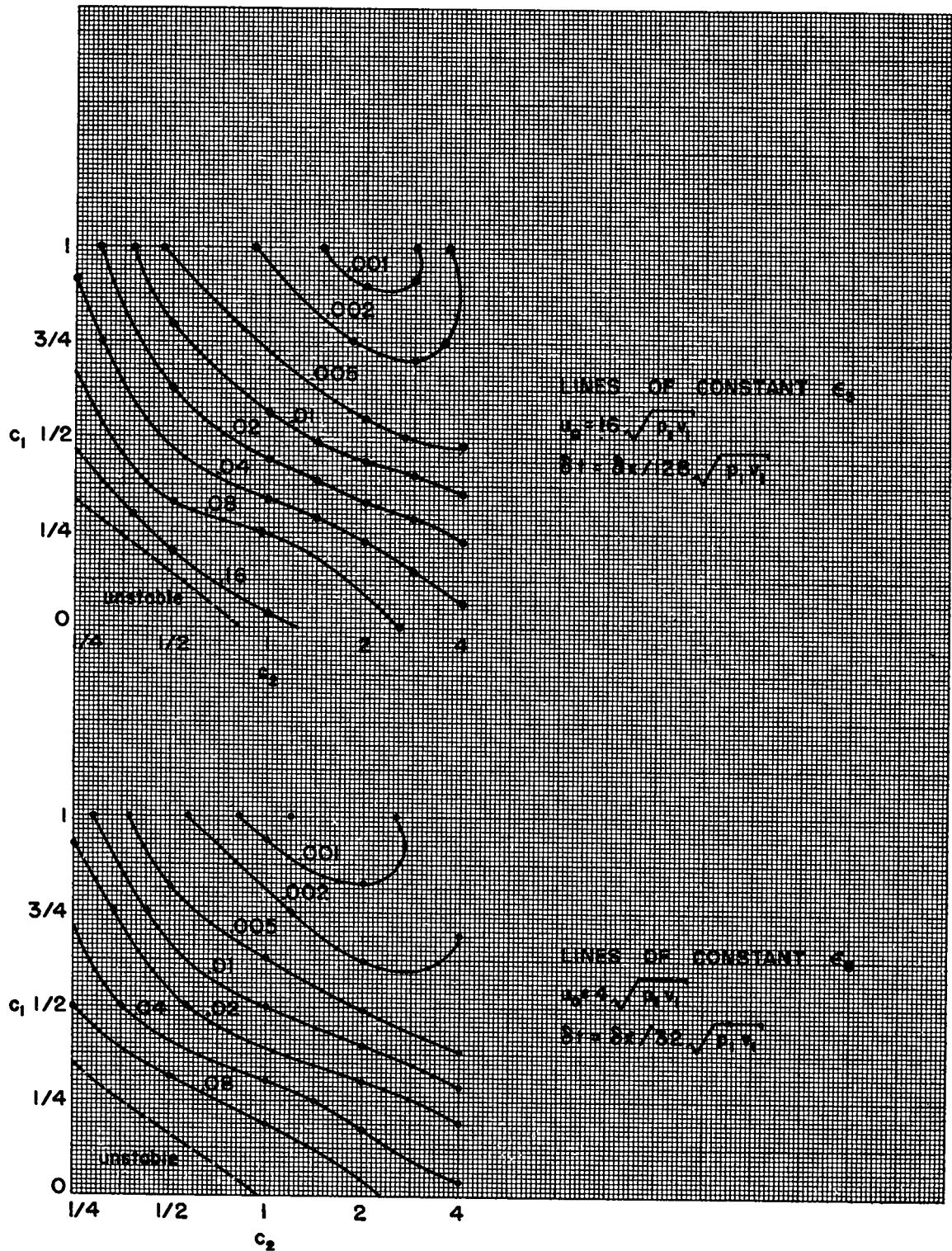


Fig. 6 Lines of constant ϵ_3 in the c_1, c_2 plane.

these can be observed in the above runs. Too much smoothing widens the shock region and it causes an overshooting of the entropy and therefore too low a density in the zone next to the piston. The origin of the first effect is obvious, and a numerical discussion for the quadratic viscosity is given in Ref. 1. Figure 7 shows how this effect depends on c_1 and c_2 for two piston velocities. No special graph is made for the pressure boundary condition (case B) because it gives the same result as comparable cases A. The second effect can be understood as follows. After a shock has travelled some distance away from the piston, it is essentially a steady state type solution as discussed in Ref. 1. One can show that the computed values of q and v are indeed close to the theoretical curve given by eq. (28) of Ref. 1:

$$qv = \frac{(\gamma + 1)}{2} M^2 (v_i - v)(v - v_f). \quad (36)$$

This relation is established irrespective of the viscosity law, provided only that there is enough viscosity to establish a steady state solution. In the first zone, on the other hand, one clearly has not the steady state type solution which gets established after the shock has run some distance away from the piston. In Fig. 8, the dependence of qv on v , as taken from an actual run, is plotted both for the first zone and for the interior zones and is compared to the theoretical expression of eq. (36).

If we rewrite eq. (18) in differential form

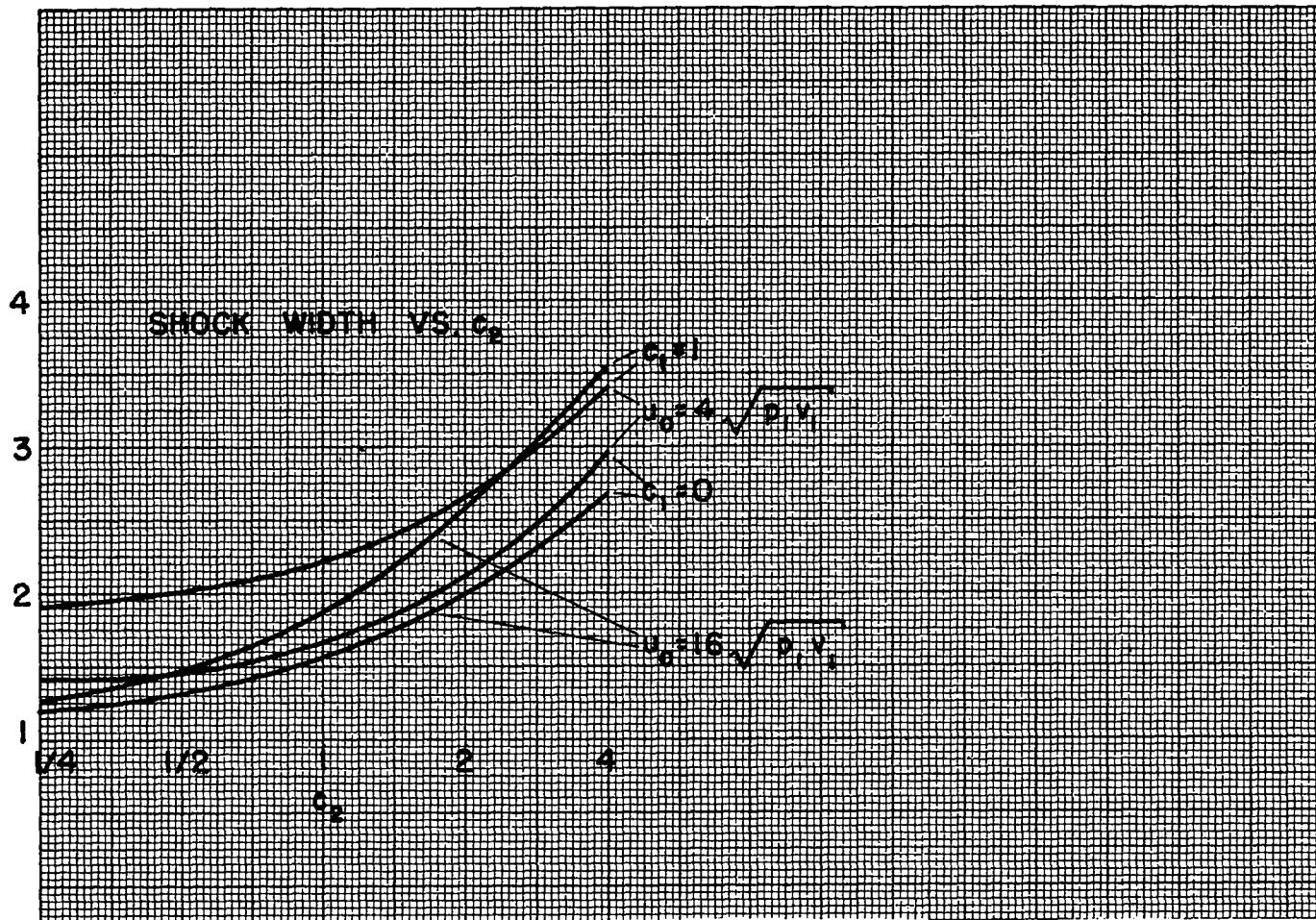


Fig. 7 Shock width vs. c_2 .

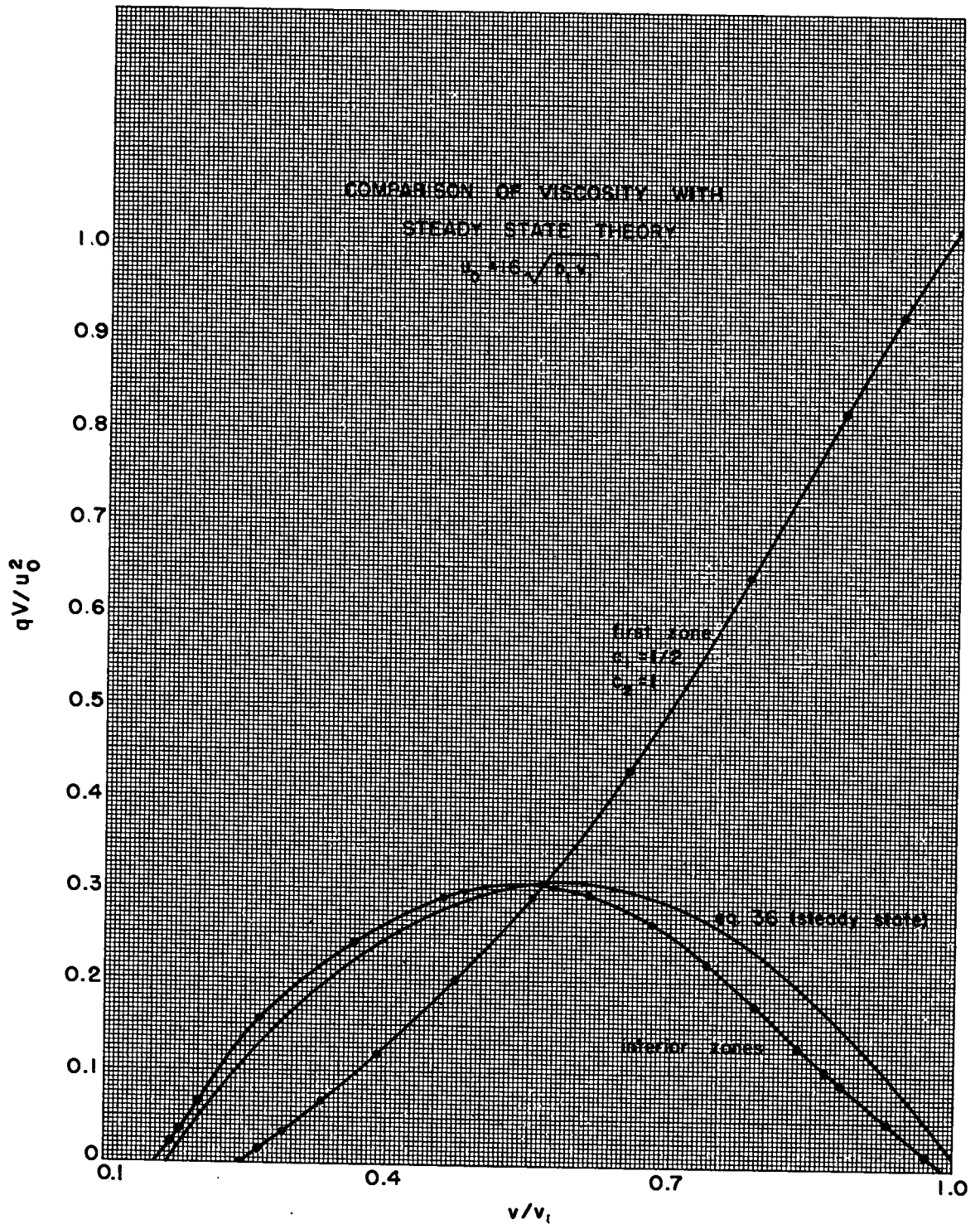


Fig. 8 Comparison of viscosity with steady state theory.

$$dE + p dV = - q dV \quad (37)$$

and multiply by the integrating factor $V^{\gamma-1}$, we obtain

$$\Delta(pV^\gamma) = - (\gamma - 1) \int qV^{\gamma-1} dV. \quad (38)$$

This relates q in a simple fashion to the entropy increase, and an inspection of Fig. 8 makes it apparent why the entropy in the first zone is too large. It is also apparent that the discrepancy grows with the amount of viscosity. Some measure of this discrepancy is the ratio of the maximum of qV in the first zone, which occurs at the very start, i.e., for $V = V_1$, to the theoretical maximum for the steady state solution as calculated from eq. (36). For small δt this ratio is

$$\frac{8}{\gamma + 1} \left(e_2 + \frac{e_1}{2} \frac{\sqrt{P_1 V_1}}{u_0} \right). \quad (39)$$

This of course makes sense only for strong shocks, because the entropy change for weak shocks is negligible anyway. In the case of Fig. 8, the contribution due to the quadratic term completely swamps the one due to the linear term. In case B, i.e., when a pressure rather than a velocity is maintained at the piston, the depression of the density of the first zone is less pronounced but nevertheless present. Fig. 9 shows the ratio of the density in the first zone, as actually obtained in some runs, to the theoretical density for the steady state solution, as function of the parameters c_1 and c_2 . There are three groups of

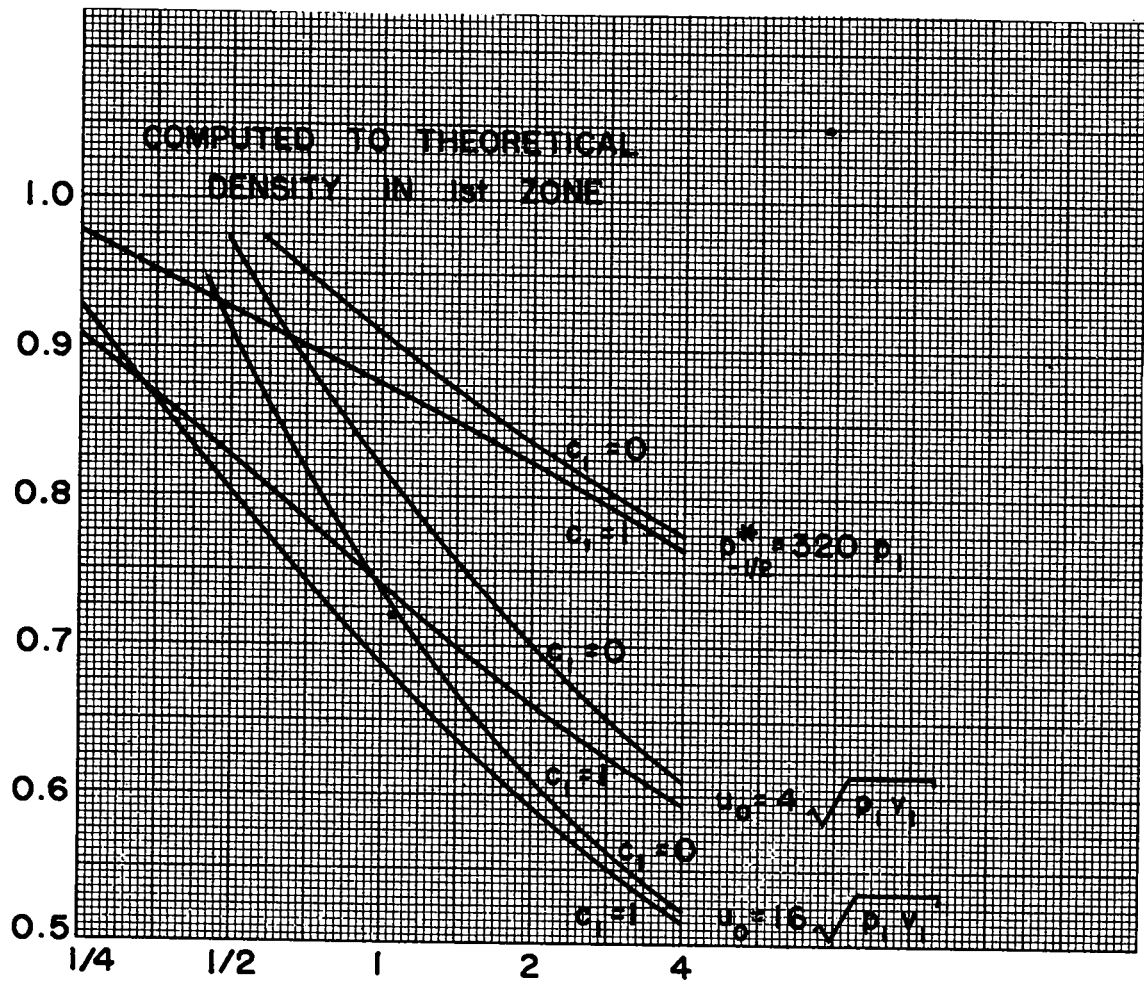


Fig. 9 Ratio of actual density in the first zone to theoretical density for the steady state solution.

curves corresponding to three different boundary conditions, two where the velocity is given and one where the pressure is given.

Figure 10 shows some density profiles (skipping the first 8 mass points) for some selected combinations of c_1 and c_2 . In both the weaker and the stronger shock curves the Courant-Friedrichs-Lewy number is about 0.4. A few runs were also made for infinitely strong shock, i.e., shocks running into a medium with $p_1 = 0$. The results were in all respects so much like the runs for which $u_0 = 16\sqrt{p_1 V_1}$ that it is not necessary to tabulate or plot them. All these data show that for the computation of flows containing a shock one does well using $c_1 = 1$, i.e., as large as possible, and $c_2 = 1/2$. This combination gives fairly good smoothing without introducing excessive troubles of the kind which were discussed just above.

The next point which was studied was the effect of viscosity pressures on the accuracy of calculating rarefaction waves (Case C). Most calculations here were made using method 2 [discussed just after eq. (21)]. In the calculations of shocks method 1 was usually employed but there is no significant difference if one uses method 2 instead because the positive Δu 's are not large enough to reach the point where q is spliced. One can see from eq. (26) that the fastest velocity with which the material will follow a receding piston is $\frac{2\sqrt{\gamma}}{\gamma-1}\sqrt{p_1 V_1}$ or, if $\gamma = 1.4$, $|u_1| = 5.916\sqrt{p_1 V_1}$. The larger one chooses $|u_0|$ the more severe a test will one have for the errors due to the viscosity pressure. Only one run was made with $u_0 = -\sqrt{p_1 V_1}$, for which a pressure

DENSITY PROFILES

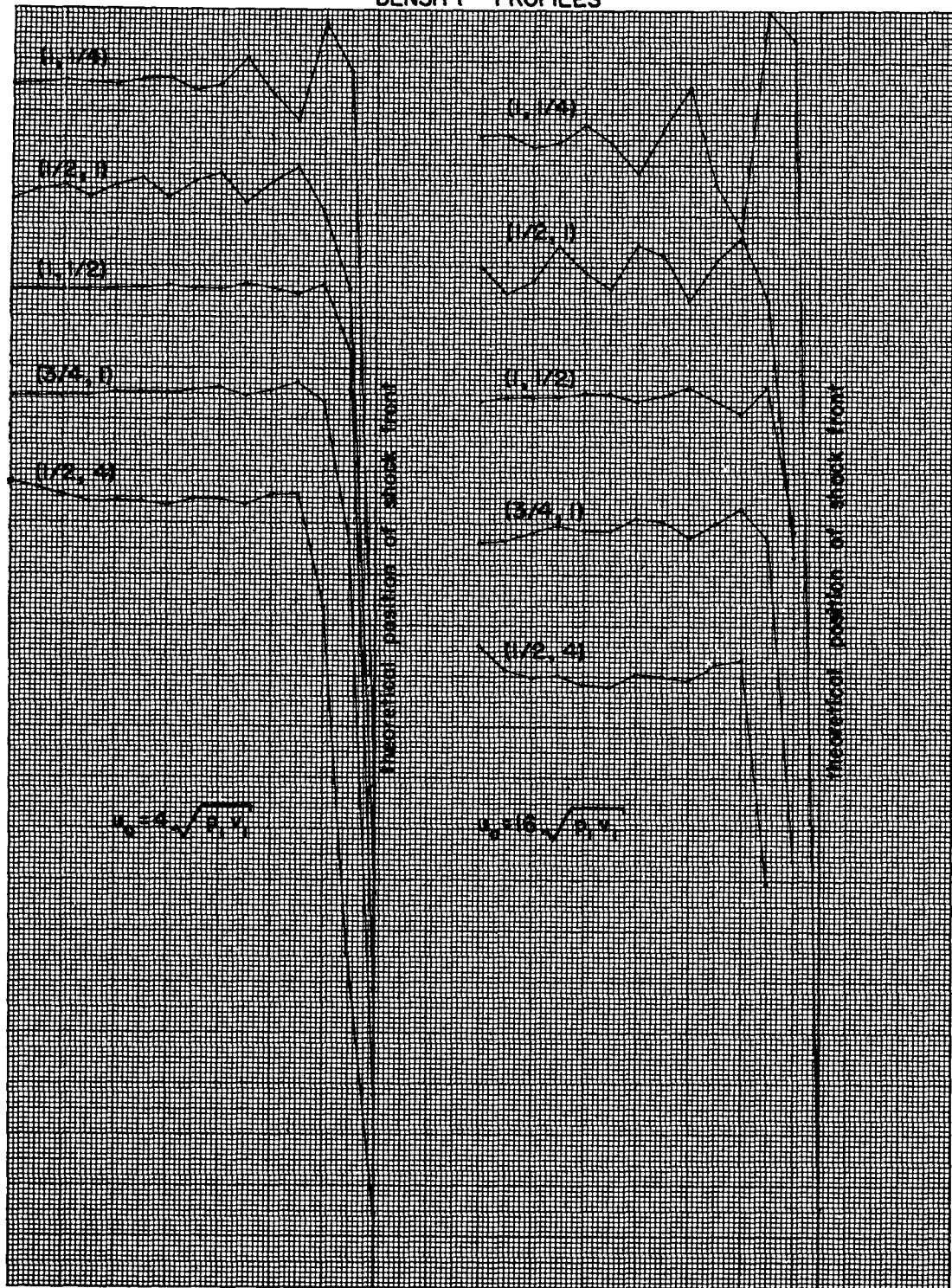


Fig. 10 Density profiles for selected combinations of c_1 and c_2 .

profile is presented in Fig. 11. The other runs were made with $u_0 = -4\sqrt{p_1 V_1}$. This is close to the limiting case of blowing off material into the vacuum and for that reason the densities and pressures at the "piston" are extremely small. Fig. 12 presents a log log plot of the density profile near the piston end of the rarefaction fan. The theoretical curve is obtained from eq. (26) for the plateau and from eq. (29) for the fan. The points are obtained from a run with $q = 0$.

The differences here are entirely due to the mesh size $\delta x = 1$, which is large compared with the Lagrange distance $x = .017$ a sound signal would have traveled on the piston side of the rarefaction fan. If one would plot the same graph on a linear scale, the differences would not show up. The points obtained from a run with $c_1 = 1$ and $c_2 = 1$ are so close to the points with $c_1 = c_2 = 0$ actually drawn in Fig. 12, that one cannot tell them apart. The difference between runs with different q does not become significant until one reaches points near the head of the rarefaction wave. Fig. 13 compares some density profiles in that range with the theoretical curve and with the curve computed with no viscosity. The agreement is now poorer for larger c_1 . It seems at first surprising that the agreement gets better for larger c_2 . This is, however, easily understood if one considers that q is levelled off for smaller Δu and at a less negative value for larger c_2 because of the use of method 2 (see Fig. 14).

The last group of problems tested the shock tube problem (case D). The initial density and pressure ratio was varied from 2:1

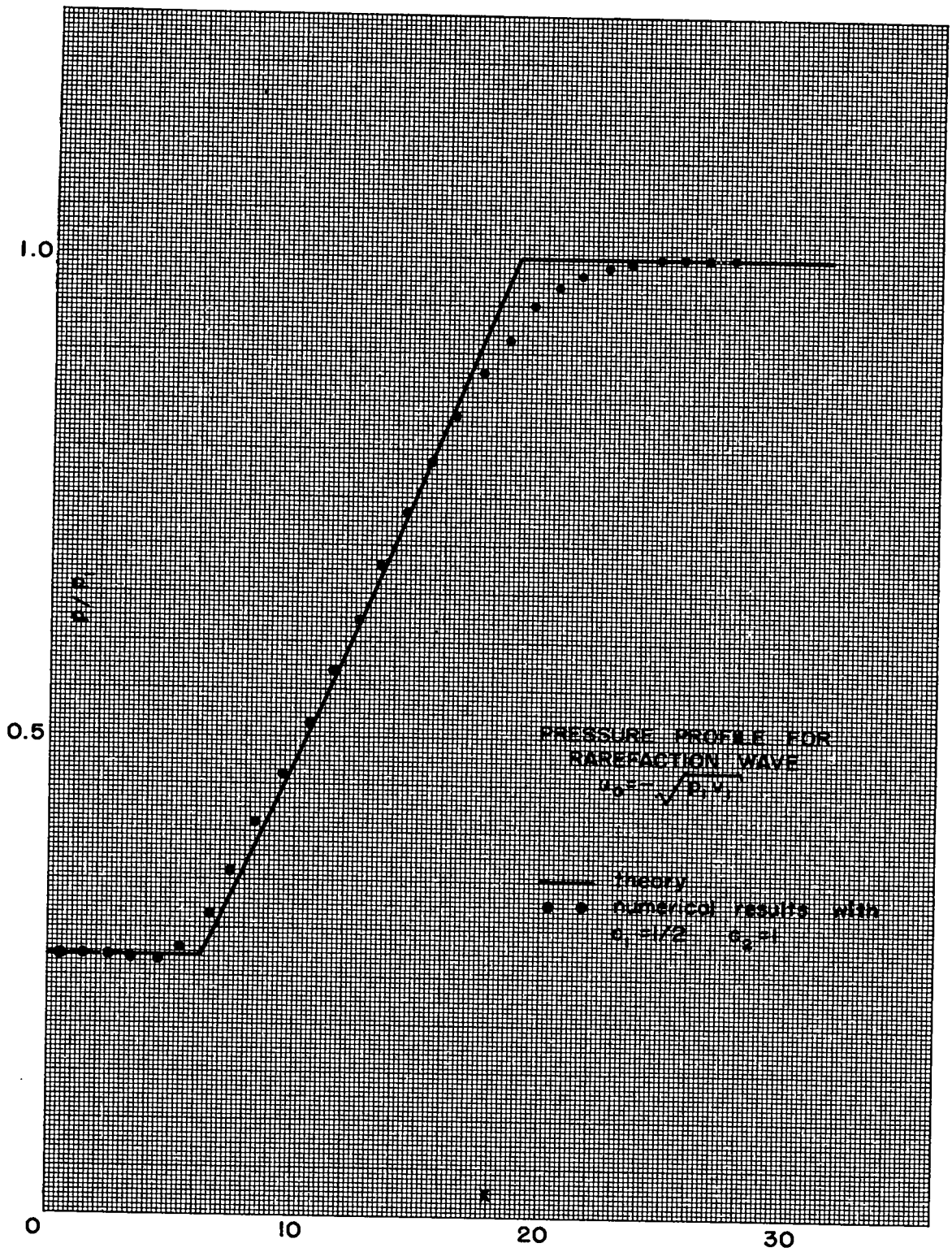


Fig. 11 Pressure profile for rarefaction wave.

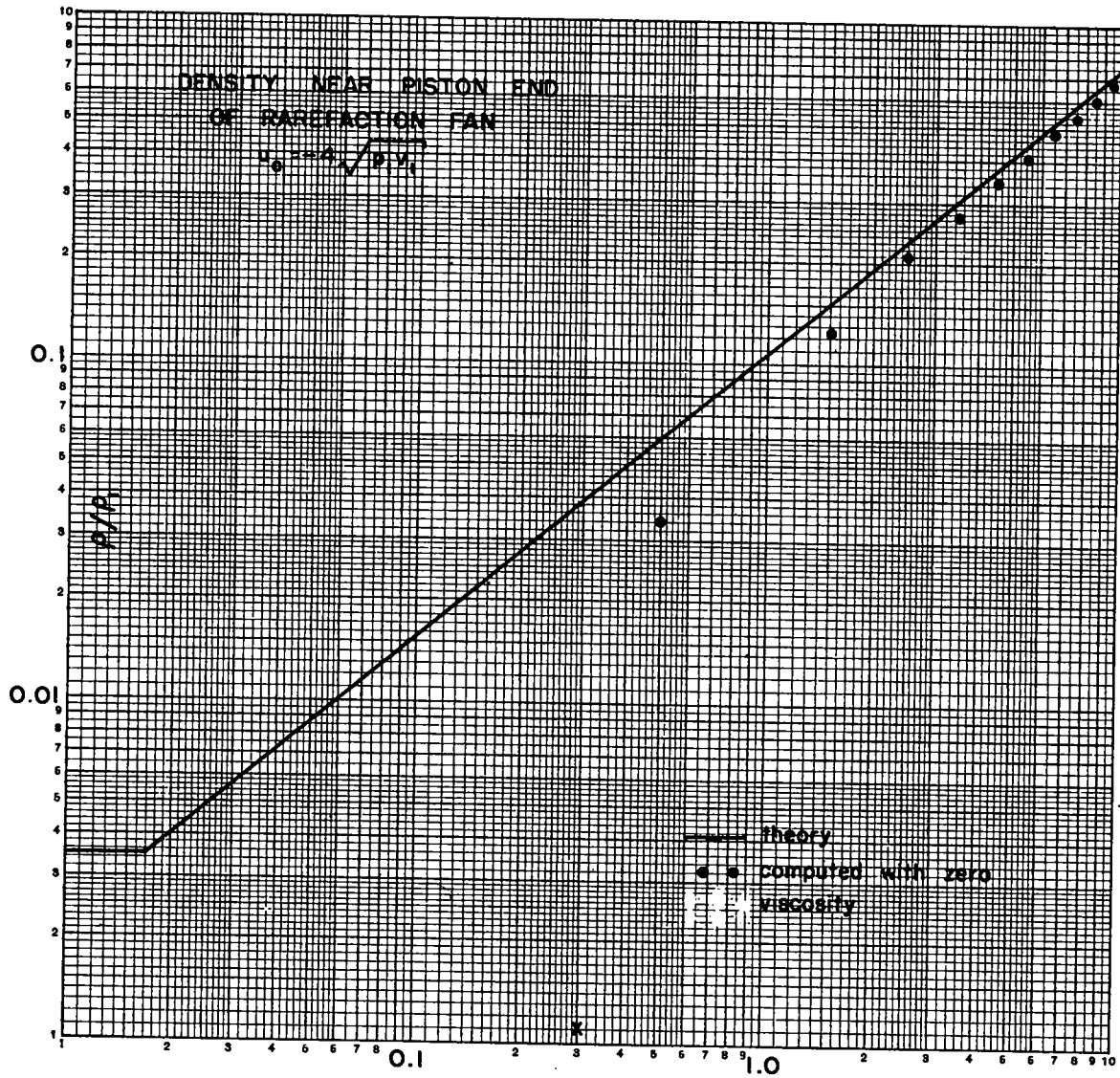


Fig. 12 Density near piston end of rarefaction fan.

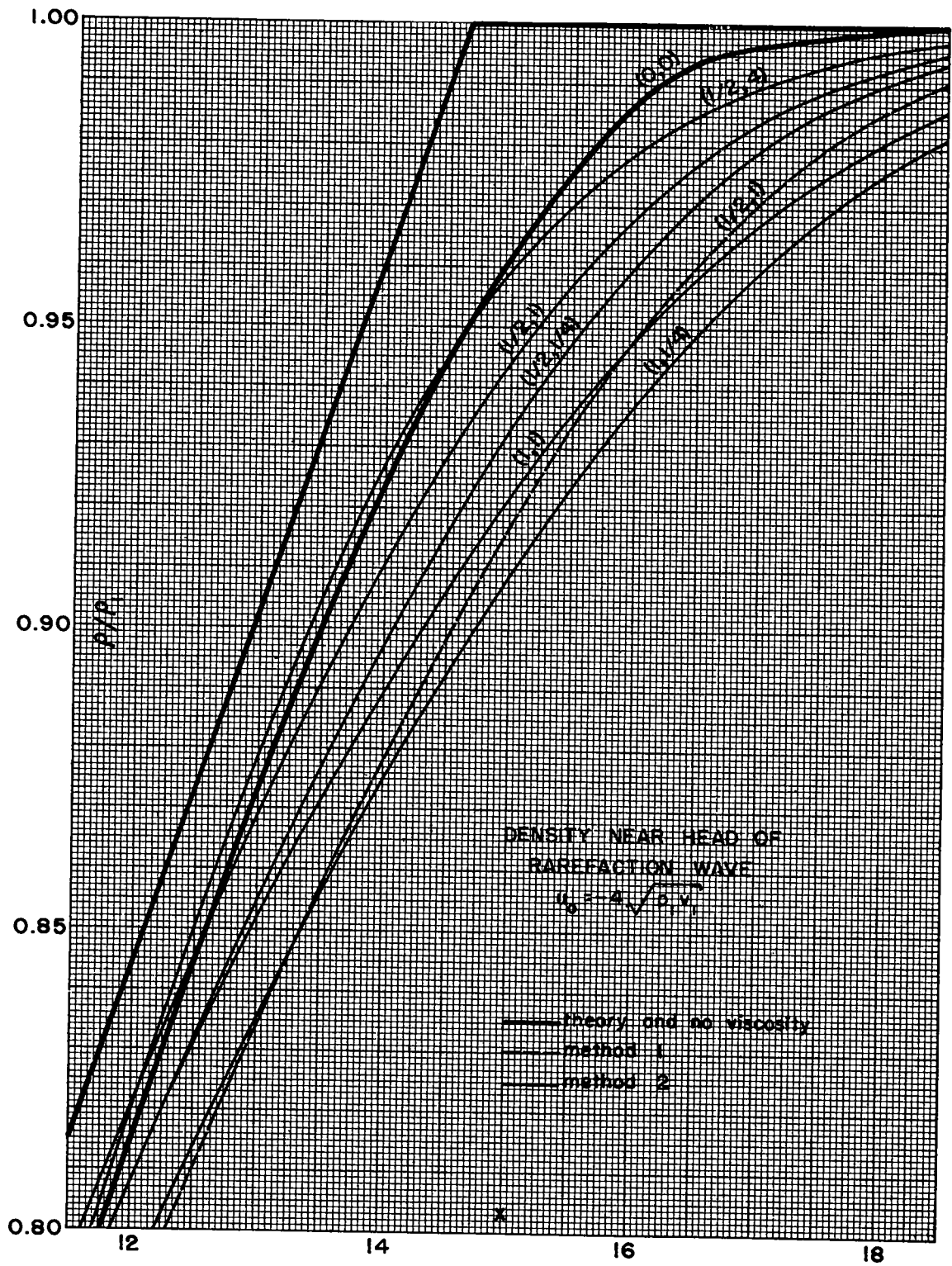


Fig. 13 Density near head of rarefaction wave.

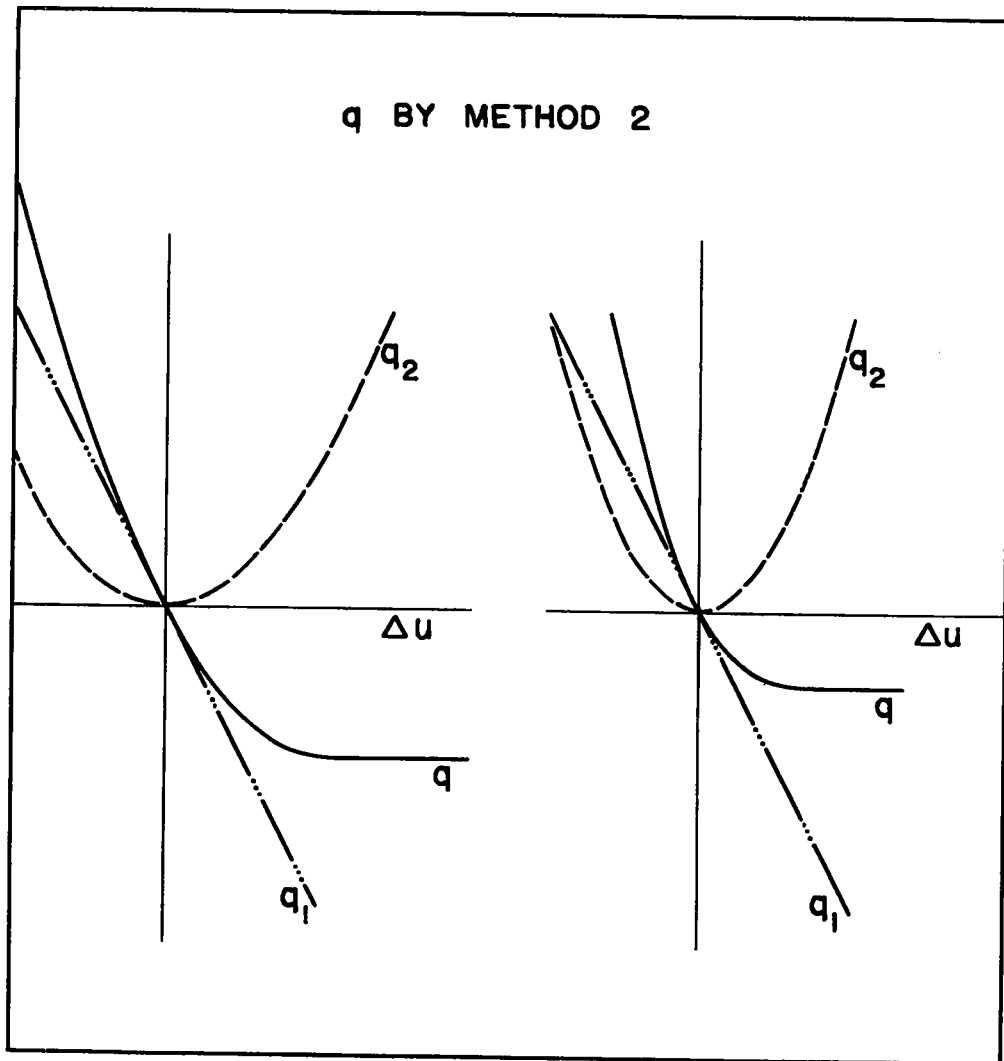


Fig. 14 Values of q determined by method 2.

to 512:1. The runs with a ratio of 2:1 were exceedingly close to the theory. Figure 15 shows a fairly typical density profile for a ratio of 32:1 compared with the theory. The quality of the approximation in the rarefaction wave agrees with the observations made on the case C runs. Figure 16 shows some runs for a ratio of 16:1 in and near the region of the density plateau (region 3 and parts of region 4 of Fig. 3). The plateau shows up much better in the runs made with method 2. In the shock region (region 2 of Fig. 3), however, method 1 is better, as evidence by Fig. 17, which presents the error of the average density and the average error of the density in that region.

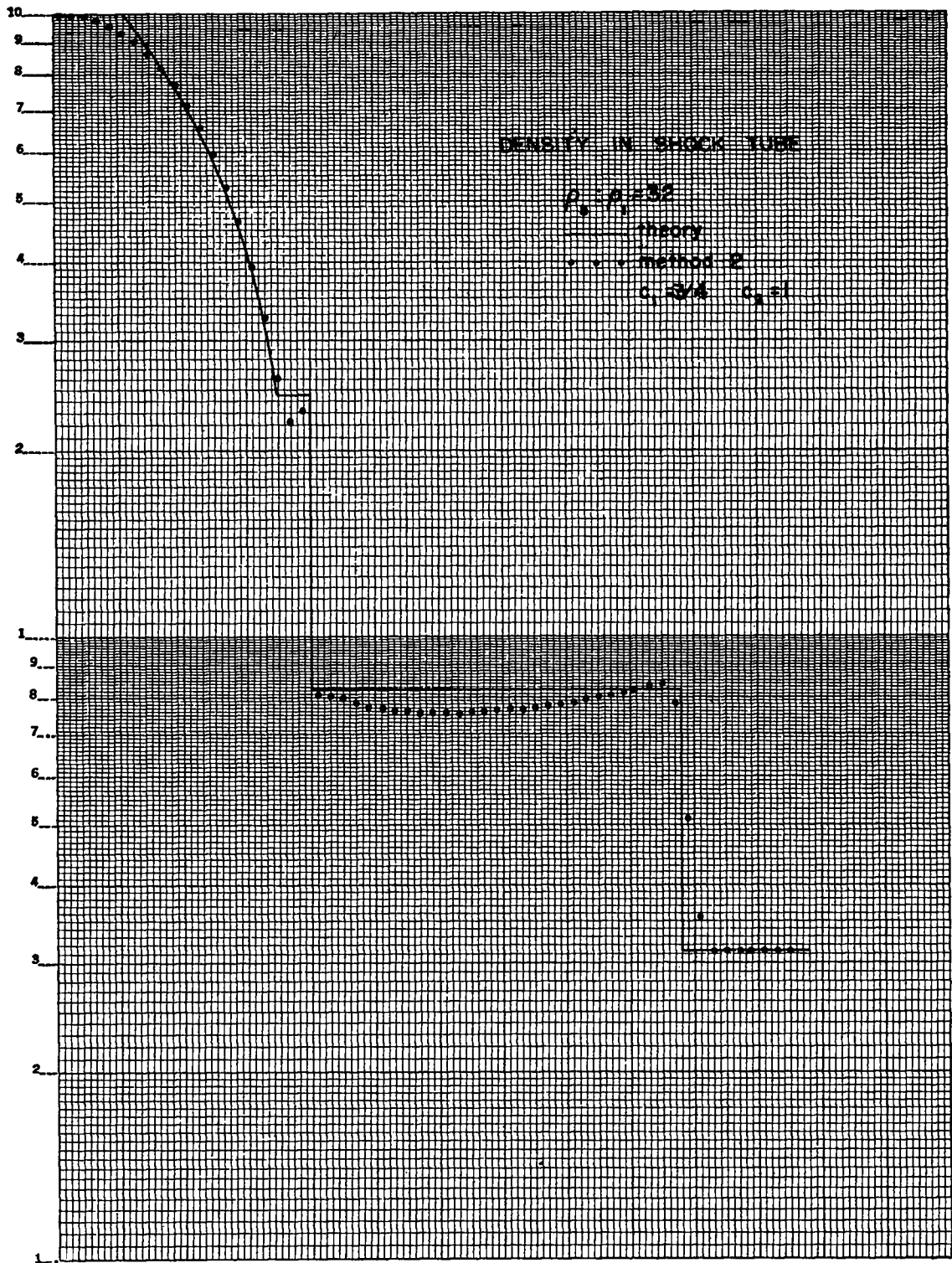


Fig. 15 Density in shock tube.

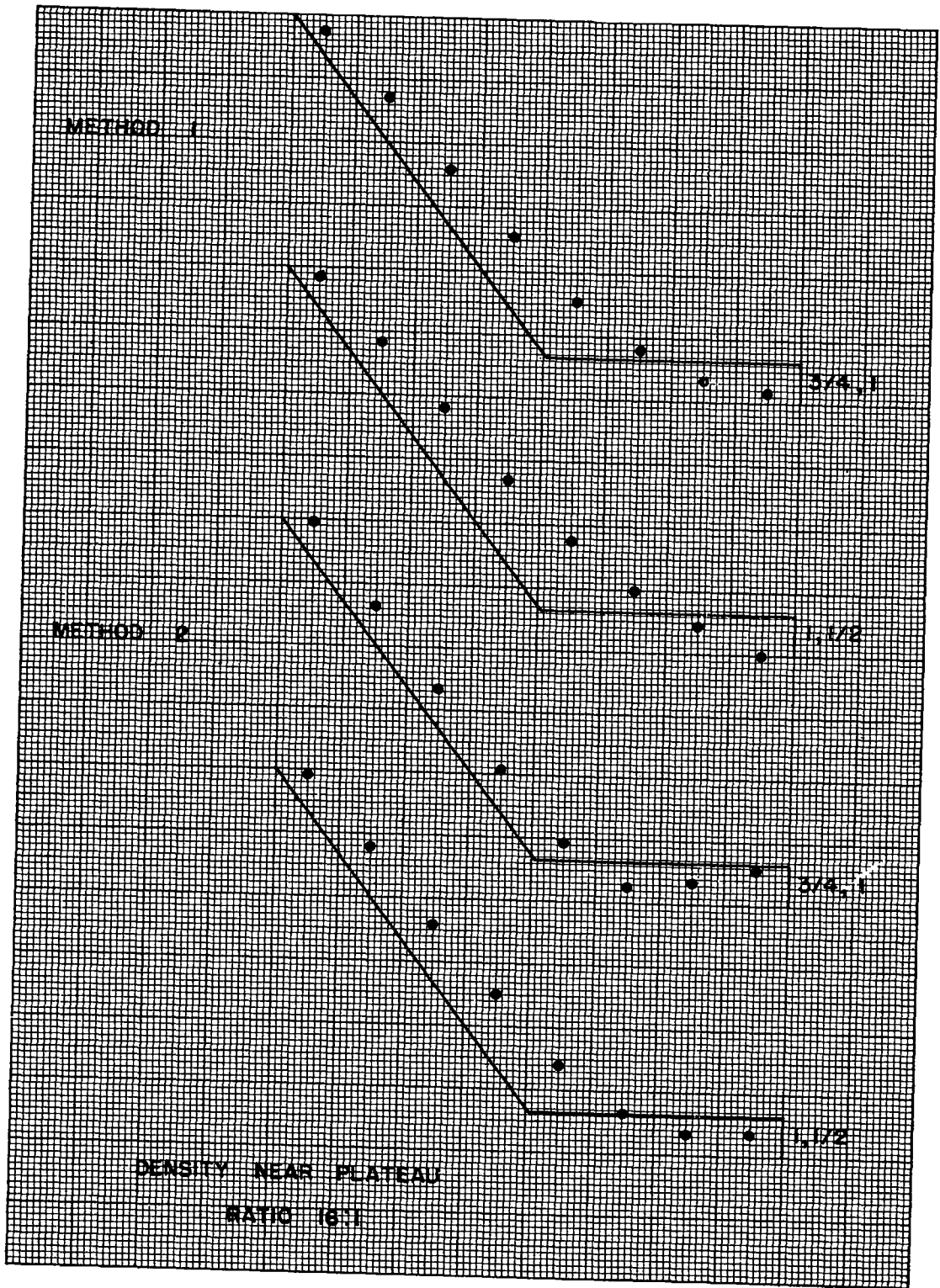


Fig. 16 Density near plateau.

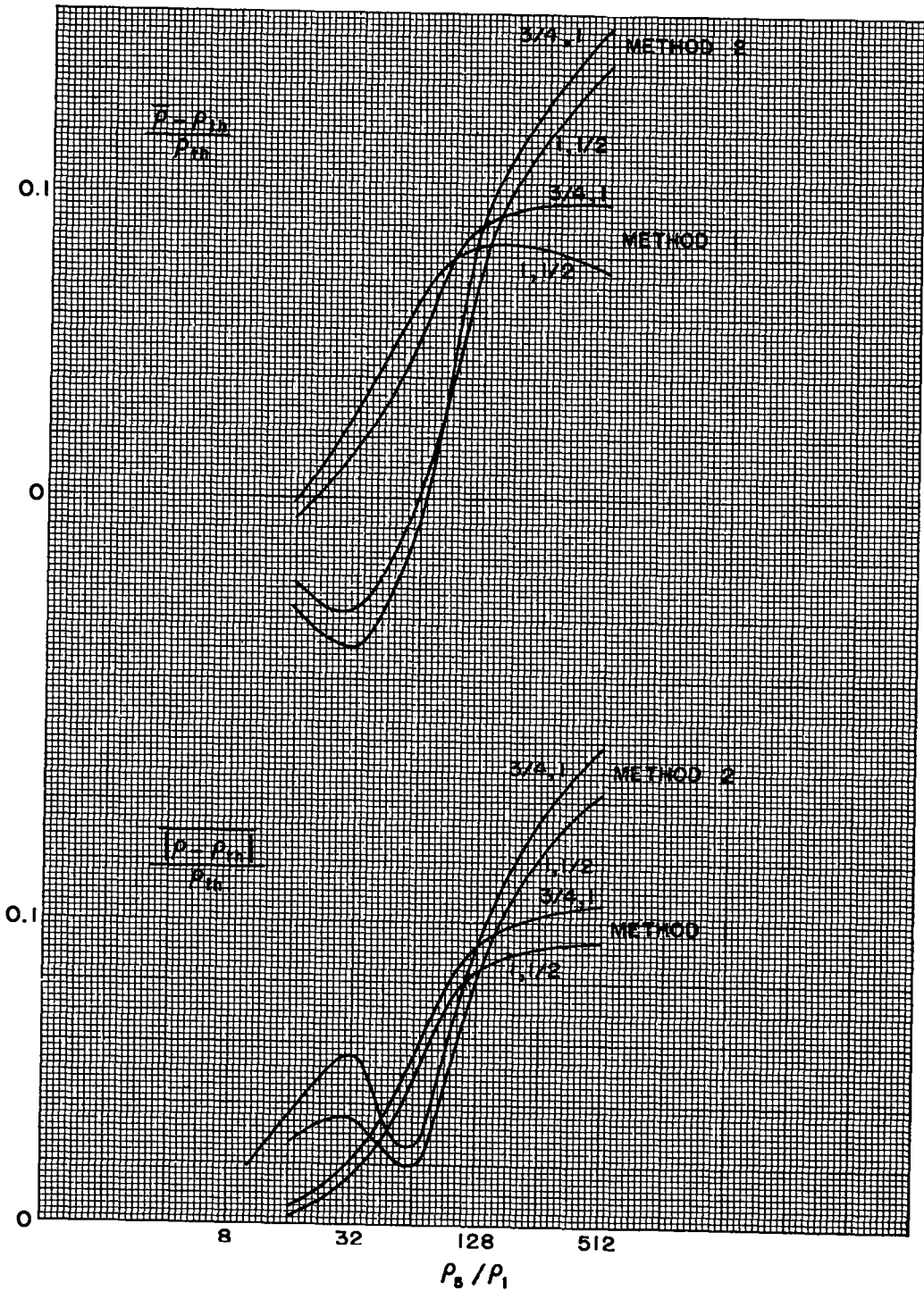


Fig. 17 Error of the average density and the average error of the density in the shock region.

REFERENCES

1. J. von Neumann and R. D. Richtmyer, J. Appl. Phys. 21, 232, 1950.
2. P. Lax, LAMS-1332, December 1952 (not available).
3. R. Courant and D. Hilbert, Methoden der Mathematischen Physik, Vol. II, Interscience, 1943.
4. R. Courant and K. O. Friedrichs, Supersonic Flow and Shock Waves, Interscience, 1948.